Tuning Nickel with Lewis Acidic Group 13 Metalloligands for Catalytic Olefin Hydrogenation

Ryan C. Cammarota and Connie C. Lu*

Department of Chemistry and Center for Metals in Biocatalysis, University of Minnesota, 207 Pleasant Street SE, Minneapolis, Minnesota 55455, United States

S *Supporting Information*

ABSTRACT: A series of bimetallic complexes pairing zero-valent nickel with group 13 M(III) ions is reported. Stronger Ni→M(III) dative bonds that render Ni more electron-deficient are seen for larger ions (In > Ga > Al). The larger Ga and In ions stabilize rare, nonclassical Ni−H$_2$ adducts that catalyze olefin hydrogenation. In contrast, neither the Ni−Al complex nor a single nickel center enables H$_2$ binding or olefin hydrogenation. By comparison of the structures, redox properties, and catalytic activities of the Ni−M series, the electronic and steric effects of the supporting metal ion are elucidated.

Bifunctional H$_2$ activation using transition metal−ligand cooperativity, e.g., via HRu−NH$_2$R, was a watershed moment in the history of asymmetric hydrogenation.[1] Metal−ligand cooperativity has become a powerful strategy to achieve base-metal-catalyzed hydrogenations.[2] Cooperativity is also inherent in the reactivity of frustrated Lewis pairs,[3] where the traditional active role of the transition metal is eschewed by main-group centers.

Recently, Lewis acidic main-group centers were shown to promote base-metal catalysis, e.g., in the hydrogenation catalyst [^{Mes}DPB^{Ph}]Ni (Figure 1).[4] Of fundamental interest is the
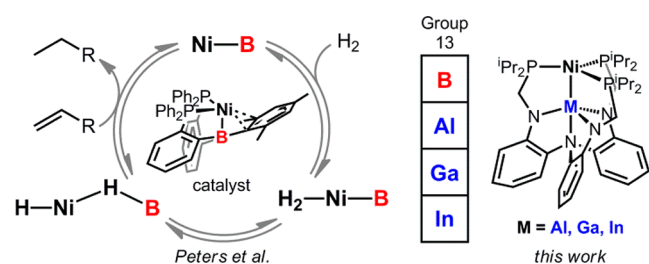

Figure 1. Nickel−group 13 catalysts for olefin hydrogenation.[4]

inverse dative bond between low-valent Ni and the Lewis acidic borane, which acts as a σ-acceptor ligand.[5] During catalysis, H$_2$ undergoes formal oxidative addition across the Ni→B bond to generate a HNi(μ-H)B intermediate, which is the active species in olefin hydrogenation.[4]

We reasoned that varying the supporting main-group metal ion might be a powerful lever to tune the reactivity at Ni. Such an approach has seldom been realized, in part because of the synthetic challenge of incorporating main-group elements into ligand scaffolds.[5b,6] The double-decker ligand N(o-(NHCH$_2$P-

(^{i}Pr)$_2$)C$_6$H$_4$)$_3$ (LH$_3$) allows the facile formation of different M(III) metalloligands, obviating the need for de novo ligand synthesis.[7] We previously reported a pair of Ni(0) complexes, NiLH$_3$ (**1**) and NiAlL (**2**). By extension to Ga(III) and In(III) supporting ions, we have created an isostructural series in which the electronic environment of Ni(0) has been systematically tuned. Ultimately, we have found that supporting Ni with the appropriate group 13 metal ion enables H$_2$ binding and catalytic olefin hydrogenation.

The Ni−M bimetallics (M = Ga, In) were prepared via a two-step metalation. Deprotonation of LH$_3$ with 3 equiv of nBuLi and subsequent addition of MCl$_3$ affords the GaL and InL metalloligands, which then react with Ni(1,5-cyclo-octadiene)$_2$ to provide NiGaL (**3**) and NiInL (**4**), respectively. The Ni(0) complexes **1**−**4** are diamagnetic and possess solution-state C_3 symmetry (Figures S1−S3). The single ^{31}P resonance of **1**−**4** (30.8, 31.3, 38.3, 45 ppm, respectively in C$_6$D$_6$) shifts downfield as the group 13 M(III) ion is introduced and varied down the group.

To prepare **4**, an argon atmosphere is necessary. Under N$_2$, the adduct species **4**-N$_2$ forms and does not revert to **4** even under prolonged vacuum. The end-on binding mode of N$_2$ was confirmed by an intense IR band at 2144 cm^{-1} in KBr (Figure S5) and X-ray crystallography (vide infra). The high ν(N−N) and short N−N bond distance of 1.103(5) Å suggest a weakly activated N$_2$ ligand. Notably, the other Ni(0) complexes **1**−**3** do not bind N$_2$. Exposure of **4**-N$_2$ to an atmosphere of H$_2$ produced **4**-H$_2$, which is stable at room temperature and does not lose H$_2$ under vacuum.

The solid-state structures of **3**, **4**, **4**-N$_2$, and **4**-H$_2$ are shown in Figure 2, and selected geometrical parameters are displayed in Table 1. The effect of the supporting M(III) ion on the solid-state structures of **1**−**4** was investigated. The M−N$_{amide}$ bond length increases linearly with the size of the M(III) ion (R^2 = 0.99; Figure S7). In contrast, the Ni−M bond lengths of 2.45, 2.38, and 2.46 Å in **2**−**4**, respectively, are surprisingly similar, especially since the M(III) ionic radius (Å) increases considerably in moving down group 13: 0.535 (Al), 0.62 (Ga), and 0.80 (In).[8]

To understand why the Ni−M bond lengths are nearly invariant in **2**−**4** despite large changes in the M(III) size, examination of the ratio (r) of the Ni−M bond distance to the sum of their respective covalent radii is instructive.[9] The r value for the Ni−M bond decreases as the supporting metal is varied
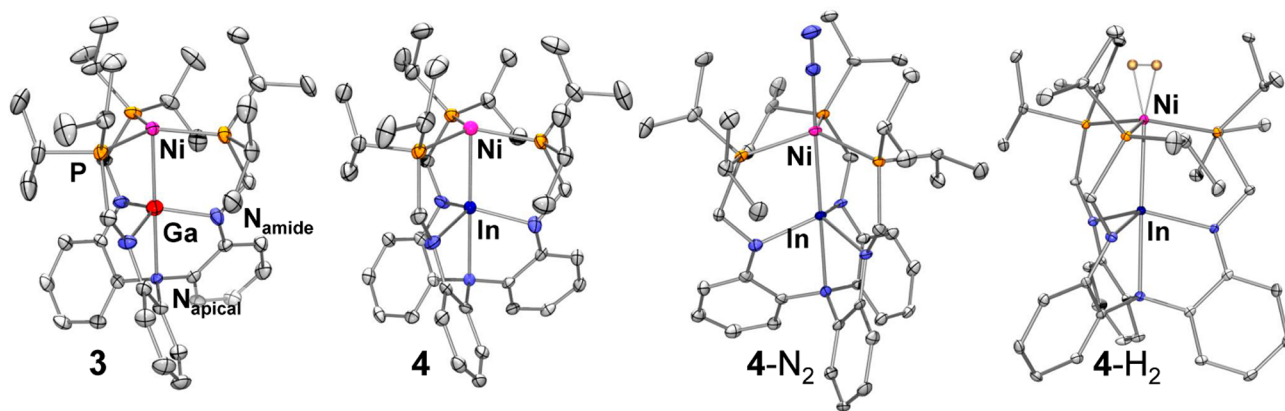
Figure 2. Solid-state structures of **3**, **4**, **4-N₂**, and **4-H₂** shown at the 50% probability level. H atoms and lattice solvent molecules have been omitted for clarity, except for H₂, which was placed from the difference map and refined with the constraint of side-on binding.

Table 1. Geometrical Parameters, Including Bond Lengths (Å) and Angles (deg), for 3, 4, 4-N₂, and 4-H₂[a]

parameter	3	4	4-N₂	4-H₂
Ni–M	2.3789(8)	2.457(1)	2.5256(7)	2.4871(3)
r[b]	0.97	0.92	0.95	0.94
Ni–P[c]	2.210(1)	2.252(1)	2.311(1)	2.265(1)
M–N$_{apical}$	2.216(3)	2.309(6)	2.385(3)	2.374(2)
M–N$_{amide}$[c]	1.954(2)	2.119(4)	2.118(2)	2.115(1)
∑P–Ni–P	359.01(9)	356.99(2)	352.06(7)	354.54(3)
∑N–M–N$_{amide}$	349.5(3)	345.3(1)	341.4(2)	343.4(1)
M to N₃ plane	0.37	0.48	0.54	0.51
Ni to P₃ plane	0.13	0.23	0.38	0.31

[a]For data for **1** and **2**, see Tables S2 and S3. [b]Ratio of the Ni–M bond length to the sum of the covalent radii.[9] [c]Average value.

down group 13: 1.00 (Al, **2**), 0.97 (Ga, **3**), and 0.92 (In, **4**). Intriguingly, r is inversely correlated with the M(III) size (R^2 = 0.98; Figure S8), which is consistent with the idea that larger, more polarizable Lewis acidic M(III) ions have better bonding overlap with Ni(0), a soft Lewis base.[10]

In addition to dictating bonding with Ni, the geometric implications of the M(III) size can be discerned by scrutinizing the Ni and M(III) binding pockets. Larger M(III) ions reside higher above the N₃ plane, from 0.26 Å for Al in **2** to 0.48 Å for In in **4** (R^2 = 0.95; Figure S9). The Ni center in **1** is essentially coplanar with the phosphine donors (Ni to P₃ plane distance = 0.03 Å). In the presence of M(III), Ni rises by 0.1 Å in **2** and **3** and by 0.2 Å in **4**, suggesting that larger M(III) ions shift Ni further above the P₃ plane. However, Ni does not rise continuously as the M(III) size increases, as it is positioned 0.13 Å above the P₃ plane in both **2** and **3** (Figure S10). Presumably, steric pressure from M(III) is counteracted by an electronic preference of Ni(0) for trigonal-planar phosphine coordination.

The Ni–P bonds elongate modestly with the addition and increasing size of M(III), from 2.18 Å in **1** to 2.25 Å in **4**, while the corresponding ³¹P resonance shifts downfield. This dual trend of Ni–P bond elongation and deshielding of the ³¹P nuclei strongly suggests that Ni→P π back-bonding decreases as M is varied down group 13. We propose that the effect is linked to the opposing gain in Ni→M dative bonding, which is reasonable because the Lewis acidic M(III) ion and the phosphine ligands compete for Ni(0) electron density. Finally, the Ni→In bond is slightly weakened upon binding of N₂ or H₂

but remains intact, as indicated by r values less than unity for both **4-N₂** and **4-H₂**.

Electrochemical studies were performed to probe the influence of the supporting group 13 metal on the electronic environment of Ni. The cyclic voltammograms for **1–3** and **4-N₂** each contain one oxidative feature, which corresponds to the Ni(I/0) redox couple (Figure 3). A reversible reduction at
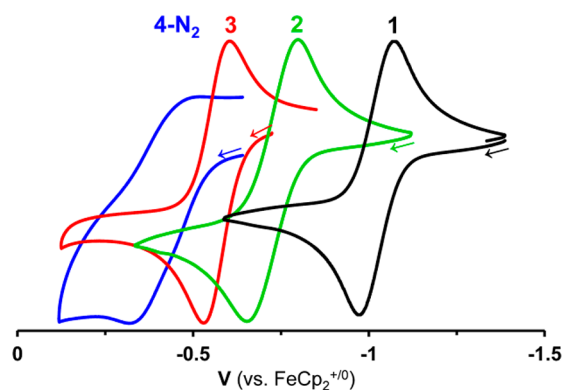

Figure 3. Cyclic voltammograms of **1–3** and **4-N₂** in 0.1 or 0.4 M [nBu₄N]PF₆ in THF at 25–50 mV/s.

−2.48 V vs FeCp₂⁺/⁰ and a quasi-reversible reduction at −2.34 V vs FeCp₂⁺/⁰ were also observed for **3** and **4-N₂**, respectively (Figure S11). For **1–3**, the oxidations at −1.02, −0.74, and −0.57 V vs FeCp₂⁺/⁰, respectively, are all fully reversible.[7] The oxidation becomes irreversible for **4-N₂**, with E_{pa} = −0.36 V vs FeCp₂⁺/⁰. Through the introduction and variation of the ancillary M(III) ion, the Ni(I/0) redox potentials shift by over 0.6 V. Notably, the Ni(I/0) redox potentials are increasingly positive for increasing ionic radius (R^2 = 0.98) or decreasing charge density (R^2 = 0.99) of the M(III) ion (Figures S12 and S13). Previously, the redox potentials of mixed-metal oxide clusters (e.g., Mn₃O₂M) were found to be linearly correlated with the Lewis acidity of the redox-inactive metal ion (M), as reflected by the pK_a of the M(H₂O)₆³⁺ species.[11] In contrast, the NiML oxidation potentials do not correlate well with pK_a,[12] pF, electronegativity, or M(III/0) reduction potential (Figures S14–S16).[8b,c] Rather, the extent of Lewis acidity exerted by group 13 ions in Ni→M species corresponds best to the M(III) size. This supports the hypothesis that larger M(III) ions have better bonding overlap with the soft Ni(0) Lewis base, thereby conferring greater Lewis acidity.

The varied electronics of the Ni centers in **1**−**4** are manifested in their reactivity with H_2. In the case of **1** and **2**, no reaction with H_2 was observed at room temperature. By contrast, exposing **3** and **4**-N_2 to 1 atm H_2 cleanly generated the Ni−H_2 adducts **3**-H_2 and **4**-H_2. Nonclassical H_2 adducts are rare—to our knowledge, only four examples of thermally stable Ni−H_2 adducts have been reported.[4b,13] Whereas **4**-H_2 is stable toward vacuum, the Ga analogue **3**-H_2 reverts back to **3**. Both **3**-H_2 and **4**-H_2 are characterized by a single ^{31}P peak at 48.5 (br) and 67.5 ppm, respectively, and a broad, unresolved ^{1}H resonance for the H_2 ligand at −2.4 and −2.5 ppm, respectively. The H−H bond is intact in **3**-H_2 and **4**-H_2, as indicated by short T_1(min) relaxation times of ≤16 and 23 ms (600 MHz), respectively (Figure S19).[14] The HD adducts exhibit $^2J_{H−D} = 34$ Hz (**3**-HD) and 32 Hz (**4**-HD) (Figures S20 and S21), which correspond to H−D distances of 0.87 and 0.91 Å, respectively (vs 0.74 Å in free H_2).[15] We propose that the stronger withdrawal of electron density from Ni by In compared with Ga necessitates increased donation from the σ bond of H_2 and consequently a slightly elongated H−H distance in **4**-H_2.

Following the H_2 binding studies, the propensity of **1**−**4** to mediate catalytic olefin hydrogenation was investigated. The hydrogenation of olefins to alkanes is a process for which few homogeneous Ni catalysts have been developed.[4a,16] Gratifyingly, **3** was catalytically competent in the hydrogenation of styrene at room temperature under 1 atm H_2 (Table 2 and

Table 2. Hydrogenation of Styrene to Ethylbenzene Mediated by 1−4[a]

entry	precatalyst	yield (%)[b]	TOF (h[−1])[c]
1	LH₃	0	0
2	NiLH₃ (**1**)	<1[d]	0
3	NiAlL (**2**)	<1	0
4	NiGaL (**3**)	>99	2.4(1)
5	NiInL (**4**)	12(5)[e]	0.10(4)

[a]Catalytic conditions: 5 mol % precatalyst, 0.087 M olefin in ca. 700 μL of C_6D_6, 1 atm H_2, room temperature. [b]Yields at 24 h for triplicate runs based on ^{1}H NMR or GC−MS analysis. [c]Turnover frequencies obtained by ^{1}H NMR analysis at >90% product or after 24 h. [d]Duplicate runs. [e]Five runs.

Figure S22). The hydrogenation of styrene was also catalyzed by **4**, albeit significantly more slowly, while **1** and **2** did not facilitate styrene hydrogenation. Catalysis by **3** was uninhibited in the presence of excess Hg, supporting a homogeneous process (see the Supporting Information).

A substrate scope study showed that **3** hydrogenates relatively unhindered olefins, e.g., 1-octene, 1-hexene, and *cis*-cyclooctene (Table 3 and Figure S23). No reaction was observed with more hindered olefins, such as *cis*-stilbene and 1,1-diphenylethylene. Likewise, internal alkenes were hydrogenated more sluggishly than terminal alkenes (cf. *trans*-2-octene vs 1-octene; Table 3). Presumably, the steric bulk of the ligand isopropyl substituents impedes the binding of hindered substrates. Unsaturated C═O and C≡C bonds, such as those in benzaldehyde and phenylacetylene, were unreactive.

While **3** hydrogenated 1-octene to octane exclusively, divergent reactivity was observed for **4** (eq 1). Under identical
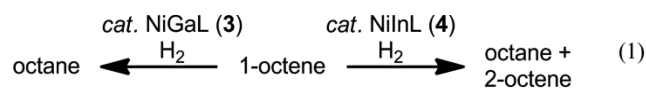

$$\text{octane} \xleftarrow[H_2]{\text{cat. NiGaL (3)}} \text{1-octene} \xrightarrow[H_2]{\text{cat. NiInL (4)}} \text{octane + 2-octene} \qquad (1)$$

Table 3. Olefin Substrate Scope for Hydrogenation Catalyzed by 3[a]

entry	substrate	yield (%)[b]	time to >90% yield (h)[b]
1	1-octene	>99	<1.5
2	1-hexene	>99	<2.75
3	styrene	>99	8
4	4-phenyl-1-butene	>99	10
5	*cis*-cyclooctene	93(3)	18
6	allyl butyl ether	68(16)	>116
7	*trans*-2-octene	10(2)	−
8	allylbenzene	3(2)	−

[a]See Table 2 for catalytic conditions and Table S4 for results with other substrates. [b]Yields at 24 h for triplicate runs based on ^{1}H NMR analysis. Hydrogenated product was exclusively formed. Several yields were confirmed by GC−MS (Table S6).

catalytic conditions, **4** converted 1-octene to 47(7)% octane and 53(7)% 2-octene in a *trans*:*cis* ratio of 4:1 (Figure S24). The isomerization of 1-octene to 2-octene requires H_2, as only trace isomerization (<2%) was observed in the absence of H_2 after 50 h (Figure S25). Similarly, the isomerization of allylbenzene to β-methylstyrene (*trans*:*cis* = 9:1) was observed to be the primary process under catalytic conditions for **4**, as β-methylstyrene and the hydrogenation product propylbenzene were formed in a 3.7:1 ratio (Table S5). The conversion of allylbenzene is significantly slower than that of 1-octene (Figure S26), as only 47(2)% consumption of allylbenzene was observed after 168 h compared with full 1-octene consumption within 20 h.

Detailed experimental and computational studies are currently underway to elucidate the mechanism and pinpoint the origin of the difference in reactivity observed for **3** and **4**. Initial mechanistic studies have allowed us to reach a few important preliminary conclusions. The necessity of H_2 for olefin isomerization suggests that it proceeds along the same mechanistic pathway as hydrogenation, with the influence of the supporting M(III) ion on Ni dictating the product outcome. Consistent with this idea, deuterium is incorporated into all three vinylic positions of free styrene under catalytic conditions with **3** and D_2 (Figure S27). This labeling study provides strong evidence that styrene inserts in both 1,2- and 2,1-fashion and that olefin insertion is reversible via β-H elimination. On the basis of the formation of 2-octene in the case of **4** but not **3**, we propose that the relative rate of reductive elimination is significantly lower for **4**, allowing β-H elimination of 2-octene to become competitive.

For all of the substrates examined, catalysis is much slower with **4** than with **3**. The catalytic resting state of **4** is **4**-H_2, which indicates that further activation of H_2 is likely the rate-determining step for **4**. The resting state of **3** was characterized by a single broad peak in the ^{31}P NMR spectrum that shifted between 41 and 47 ppm depending on the olefin substrate (Table S7). Upon cooling to −50 °C in toluene-d_8, **3**-H_2 was observed as the resting state. We speculate that olefin reversibly binds to **3**-H_2 in fast equilibrium at room temperature. Additionally, a normal primary kinetic isotope effect of 1.7(2) was measured for the hydrogenation of styrene by **3**, which suggests that H−H bond cleavage is involved in the rate-determining step.

After H−H bond activation, the intermediacy of a HNi(μ-H)M species is presumed, analogous to [$^{Mes}DPB^{Ph}$](μ-H)NiH.[4] Although we have not observed such a species, it is reasonable

that differences in catalytic activity between **3** and **4** reflect their different propensities to stabilize a HNi(μ-H)M intermediate, as M−H bonds are destabilized going down group 13.[17] In the [^{Mes}DPB^{Ph}]Ni system, no H$_2$ adduct was observed, but a small modification of the ligand, [^{Ph}DPB^{iPr}], allowed both the H$_2$ adduct and HNi(μ-H)B species to be observed.[4] We propose that one effect of a larger M(III) ion is to shift the equilibrium between (H$_2$)Ni→M and HNi(μ-H)M in favor of the H$_2$ adduct. Consistent with this proposal, addition of a 1:1 H$_2$/D$_2$ mixture to **3** and **4** in the absence of olefin did not result in any observable formation of HD, which stands in contrast to the rapid formation of HD upon addition of such a mixture to [^{Mes}DPB^{Ph}]Ni (Figure S28).[4a]

In closing, the electrochemical and structural data reveal that larger group 13 M(III) ions withdraw more electron density from Ni and force Ni higher above the P$_3$ plane, both of which render Ni more poised to bind small molecules such as N$_2$ and H$_2$. Catalytic hydrogenation activity, however, does not strictly improve with larger M(III), as styrene hydrogenation with NiGaL is 24 times faster than that with NiInL. Future studies will investigate the mechanistic pathway to better understand the role of the supporting metal in catalysis.

■ ASSOCIATED CONTENT

Ⓢ Supporting Information

The Supporting Information is available free of charge on the ACS Publications website at DOI: 10.1021/jacs.5b08313.

> X-ray crystallographic data for **3**, **4**, **4**-N$_2$, and **4**-H$_2$ (CIF)
> Experimental procedures and physical data (PDF)

The X-ray crystallographic data have also been deposited in the CCDC database (1402134−1402137).

■ AUTHOR INFORMATION

Corresponding Author

*clu@umn.edu

Notes

The authors declare no competing financial interest.

■ ACKNOWLEDGMENTS

■ REFERENCES

(1) (a) Noyori, R.; Kitamura, M.; Ohkuma, T. *Proc. Natl. Acad. Sci. U. S. A.* **2004**, *101*, 5356−5362. (b) Noyori, R.; Sandoval, C. A.; Muñiz, K.; Ohkuma, T. *Philos. Trans. R. Soc., A* **2005**, *363*, 901−912.

(2) (a) Chirik, P. J. In *Catalysis without Precious Metals*; Bullock, R. M., Ed.; Wiley-VCH: Weinheim, Germany, 2010; p 83. (b) Casey, C. P.; Guan, H. *J. Am. Chem. Soc.* **2007**, *129*, 5816−5817. (c) Zuo, W. W.; Lough, A. J.; Li, Y. F.; Morris, R. H. *Science* **2013**, *342*, 1080−1083. (d) Morris, R. H. *Acc. Chem. Res.* **2015**, *48*, 1494−1502. (e) Langer, R.; Leitus, G.; Ben-David, Y.; Milstein, D. *Angew. Chem., Int. Ed.* **2011**, *50*, 2120−2124. (f) Zhang, G.; Vasudevan, K. V.; Scott, B. L.; Hanson, S. K. *J. Am. Chem. Soc.* **2013**, *135*, 8668−8681. (g) Chirik, P. J. *Acc. Chem. Res.* **2015**, *48*, 1687−1695.

(3) (a) Stephan, D. W.; Greenberg, S.; Graham, T. W.; Chase, P.; Hastie, J. J.; Geier, S. J.; Farrell, J. M.; Brown, C. C.; Heiden, Z. M.; Welch, G. C.; Ullrich, M. *Inorg. Chem.* **2011**, *50*, 12338−12348.

(b) Hounjet, L. J.; Stephan, D. W. *Org. Process Res. Dev.* **2014**, *18*, 385−391.

(4) (a) Harman, W. H.; Peters, J. C. *J. Am. Chem. Soc.* **2012**, *134*, 5080−5082. (b) Harman, W. H.; Lin, T.-P.; Peters, J. C. *Angew. Chem., Int. Ed.* **2014**, *53*, 1081−1086.

(5) (a) Amgoune, A.; Bourissou, D. *Chem. Commun.* **2011**, *47*, 859−871. (b) Sircoglou, M.; Bontemps, S.; Bouhadir, G.; Saffon, N.; Miqueu, K.; Gu, W.; Mercy, M.; Cheng, C.-H.; Foxman, B. M.; Maron, L.; Ozerov, O. V.; Bourissou, D. *J. Am. Chem. Soc.* **2008**, *130*, 16729−16738.

(6) (a) Derrah, E. J.; Sircoglou, M.; Mercy, M.; Ladeira, S.; Bouhadir, G.; Miqueu, K.; Maron, L.; Bourissou, D. *Organometallics* **2011**, *30*, 657−660. (b) Sircoglou, M.; Mercy, M.; Saffon, N.; Coppel, Y.; Bouhadir, G.; Maron, L.; Bourissou, D. *Angew. Chem., Int. Ed.* **2009**, *48*, 3454−3457. (c) Burlitch, J. M.; Leonowicz, M. E.; Petersen, R. B.; Hughes, R. E. *Inorg. Chem.* **1979**, *18*, 1097−1105.

(7) (a) Rudd, P. A.; Liu, S.; Gagliardi, L.; Young, V. G.; Lu, C. C. *J. Am. Chem. Soc.* **2011**, *133*, 20724−20727. (b) Clouston, L. J.; Siedschlag, R. B.; Rudd, P. A.; Planas, N.; Hu, S.; Miller, A. D.; Gagliardi, L.; Lu, C. C. *J. Am. Chem. Soc.* **2013**, *135*, 13142−13148.

(8) (a) Shannon, R. D. *Acta Crystallogr., Sect. A: Cryst. Phys., Diffr., Theor. Gen. Crystallogr.* **1976**, *32*, 751−767. (b) Downs, A. J. *Chemistry of Aluminum, Gallium, Indium, and Thallium*; Chapman & Hall: London, 1993. (c) Christe, K. O.; Dixon, D. A.; McLemore, D.; Wilson, W. W.; Sheehy, J. A.; Boatz, J. A. *J. Fluorine Chem.* **2000**, *101*, 151−153.

(9) Cordero, B.; Gómez, V.; Platero-Prats, A. E.; Revés, M.; Echeverría, J.; Cremades, E.; Barragán, F.; Alvarez, S. *Dalton Trans.* **2008**, 2832−2838.

(10) (a) Pearson, R. G. *J. Am. Chem. Soc.* **1963**, *85*, 3533−3539. (b) Sivaev, I. B.; Bregadze, V. I. *Coord. Chem. Rev.* **2014**, *270−271*, 75−88.

(11) (a) Tsui, E. Y.; Tran, R.; Yano, J.; Agapie, T. *Nat. Chem.* **2013**, *5*, 293−299. (b) Herbert, D. E.; Lionetti, D.; Rittle, J.; Agapie, T. *J. Am. Chem. Soc.* **2013**, *135*, 19075−19078. (c) Tsui, E. Y.; Agapie, T. *Proc. Natl. Acad. Sci. U. S. A.* **2013**, *110*, 10084−10088.

(12) The nature of the Lewis acid−base interactions is distinctly different: Ni→M versus Mn−O→M in the Mn$_3$O$_2$M clusters.

(13) (a) Connelly, S. J.; Zimmerman, A. C.; Kaminsky, W.; Heinekey, D. M. *Chem. - Eur. J.* **2012**, *18*, 15932−15934. (b) Tsay, C.; Peters, J. C. *Chem. Sci.* **2012**, *3*, 1313−1318. (c) Kubas, G. J. *Chem. Rev.* **2007**, *107*, 4152−4205.

(14) Desrosiers, P. J.; Cai, L.; Lin, Z.; Richards, R.; Halpern, J. *J. Am. Chem. Soc.* **1991**, *113*, 4173−4184.

(15) Luther, T. A.; Heinekey, D. M. *Inorg. Chem.* **1998**, *37*, 127−132.

(16) (a) Vasudevan, K. V.; Scott, B. L.; Hanson, S. K. *Eur. J. Inorg. Chem.* **2012**, *2012*, 4898−4906. (b) Lin, T.-P.; Peters, J. C. *J. Am. Chem. Soc.* **2014**, *136*, 13672−13683. (c) Mooibroek, T. J.; Wenker, E. C. M.; Smit, W.; Mutikainen, I.; Lutz, M.; Bouwman, E. *Inorg. Chem.* **2013**, *52*, 8190−8201.

(17) Aldridge, S.; Downs, A. J. *Chem. Rev.* **2001**, *101*, 3305−3365.